Distinguishing Coherent and Thermal Photon Noise in a Circuit Quantum Electrodynamical System

Fei Yan,[1,*] Dan Campbell,[1] Philip Krantz,[1] Morten Kjaergaard,[1] David Kim,[2] Jonilyn L. Yoder,[2] David Hover,[2] Adam Sears,[2] Andrew J. Kerman,[2] Terry P. Orlando,[1] Simon Gustavsson,[1] and William D. Oliver[1,2,3]

[1]*Research Laboratory of Electronics, Massachusetts Institute of Technology, Cambridge, Massachusetts 02139, USA*
[2]*MIT Lincoln Laboratory, 244 Wood Street, Lexington, Massachusetts 02420, USA*
[3]*Department of Physics, Massachusetts Institute of Technology, Cambridge, Massachusetts 02139, USA*

(Received 1 January 2018; published 29 June 2018)

In the cavity-QED architecture, photon number fluctuations from residual cavity photons cause qubit dephasing due to the ac Stark effect. These unwanted photons originate from a variety of sources, such as thermal radiation, leftover measurement photons, and cross talk. Using a capacitively shunted flux qubit coupled to a transmission line cavity, we demonstrate a method that identifies and distinguishes coherent and thermal photons based on noise-spectral reconstruction from time-domain spin-locking relaxometry. Using these measurements, we attribute the limiting dephasing source in our system to thermal photons rather than coherent photons. By improving the cryogenic attenuation on lines leading to the cavity, we successfully suppress residual thermal photons and achieve T_1-limited spin-echo decay time. The spin-locking noise-spectroscopy technique allows broad frequency access and readily applies to other qubit modalities for identifying general asymmetric nonclassical noise spectra.

DOI: 10.1103/PhysRevLett.120.260504

Superconducting cavity modes are widely used in quantum information processing for mediating two-qubit interactions, reading out qubits, storing information, and even acting as qubits [1–4]. Each added cavity can also introduce additional channels for qubit relaxation and dephasing [5–8]. For example, photon number fluctuations in the cavity cause qubit dephasing due to a photon-number-dependent frequency shift of the qubit, the ac Stark effect, which is considered a major source of decoherence in state-of-the-art systems [9]. For cooling or resetting cavities [10–12], it remains challenging to identify and suppress unwanted cavity photons at the level demanded by fault-tolerant applications. These residual cavity photons arise from a variety of sources, e.g., thermal microwave photons from blackbody radiation that is improperly attenuated or filtered in the cryogenic environment [13]. Additionally, unwanted coherent photons can remain in the cavity following readout [5,14] or from microwave cross talk in a multiqubit system. The distinction between thermal and coherent photons has been measured by either spectroscopically resolving photon-number states of the qubit [15,16] or by characterizing the dependence of qubit dephasing on the mean photon number $\bar{n}$ [17] in the regime where qubit-cavity dispersive coupling χ is much stronger than the photon loss rate κ and where the mean photon number is sufficiently large ($\bar{n} \gtrsim 1$). However, in the operating regime more relevant to quantum information processing applications, where the coupling is relatively weak ($2\chi \lesssim \kappa$) and the residual photon number is small ($\bar{n} \ll 1$), it becomes challenging to differentiate photons from uncontrollable coherent and thermal sources.

An alternative approach to characterizing and identifying a random process is the direct measurement of its power spectral densities (PSDs). There are several ways to perform noise spectroscopy [18–24], depending on the frequency range of interest and the system properties. To measure noise within a band of 0.1–100 MHz, which is relevant to dephasing in superconducting qubits, the spin-locking—also called $T_{1\rho}$—noise-spectroscopy technique was demonstrated in our previous works [9,25] and proved to be advantageous, because it takes advantage of robustness against low-frequency noise that is inherent in driven evolution and it features a relatively straightforward relaxometry analysis with fewer assumptions than free-evolution techniques [21]. However, the previous works were limited to classical spectra, and a general nonclassical spectrum—evident as an asymmetric noise spectrum with respect to zero frequency [26]—has not yet been demonstrated in the classical equilibrium limit ($\hbar\omega \ll k_B T$, where T is the temperature; typically, $T \approx 50$ mK for superconducting qubits). We note that such an asymmetric spectrum has recently been measured in the large-frequency regime (≥ 1 GHz) [27]. Developing such a complete characterization technique enables studies with both fundamental and practical significance, e.g., for metrology, nonequilibrium dynamics, qubit noise correlations, and environmental engineering [28]. The spin-locking protocol has also been demonstrated in coherence characterization [29], active cooling [30], and magnetic sensing [31].

In this Letter, we extend the spin-locking noise-spectroscopy technique to the case of nonclassical (two-sided, emission and absorption) noise spectra and demonstrate it with engineered coherent and thermal photon noise. To the qubit, the engineered noise photons generated by a coherent source exhibit a Lorentzian-shaped spectrum centered at the frequency detuning between the cavity and the drive. Such an asymmetric spectrum is clearly traceable to the nonequilibrium, engineered-noise environment, even when the system is operated in the classical equilibrium (low-frequency) limit. The spectral width of coherent photon noise is half that of the corresponding spectral width for thermal photons, due to the difference in their correlation times. Using this technique, we find that the photon noise limiting our qubit dephasing originates from thermal sources. By improving the cryogenic attenuation in our experiment, we obtain a spin-echo decay time $T_{2\mathrm{Echo}}$ near the $2T_1$ limit.

Our test device [Fig. 1(a)] is a superconducting capacitively shunted flux qubit (CSFQ) embedded in a coplanar transmission line cavity. Details about the design and fabrication of this device can be found in Ref. [9]. The sample is tested in a dilution refrigerator at a base temperature of 20 mK. The cavity, which is symmetrically overcoupled at the input and output port, has a center frequency $\omega_c/2\pi \approx 8.26$ GHz and decay rate $\kappa/2\pi \approx 1.69$ MHz. The qubit is biased at its flux-insensitive point (transition frequency $\omega_q/2\pi \approx 3.70$ GHz) and is capacitively coupled to the cavity, resulting in an effective dispersive coupling between the qubit and cavity (coupling strength $\chi/2\pi \approx 0.31$ MHz). An rf signal (ω_{ro}) near the cavity frequency is used to read out the qubit state [Fig. 1(b)]. Within the rotating-wave approximation [25,30], a qubit drive (ω_{qb}) creates an effective two-level system in the rotating frame with a transition frequency equivalent to the Rabi frequency Ω. The Hamiltonian with a resonant qubit drive ($\omega_{qb} = \omega_q$) can be expressed as

$$H/\hbar = \Omega\hat{\sigma}_z/2 + \chi\hat{a}^\dagger\hat{a}\hat{\sigma}_x + \omega_c\hat{a}^\dagger\hat{a}, \tag{1}$$

where $\hat{\sigma}_z$ is the Pauli operator in the new eigenbasis defined by the Rabi drive field and $\hat{a}^\dagger$ ($\hat{a}$) is the cavity photon creation (annihilation) operator. The photon number operator is then $\hat{n} = \hat{a}^\dagger\hat{a}$. Equation (1) indicates that photon number fluctuations—the same noise that dephases the original qubit in the lab frame—now transversely couple to the dressed qubit and result in an energy exchange. This shows that a random process may affect a quantum system differently depending on the control protocol. Considering only lab-frame relaxation processes (relaxation rate $\Gamma_1 = 1/T_1$) and photon noise, we can relate the dressed qubit's relaxation and emission rates, $\Gamma_{\downarrow\rho}$ and $\Gamma_{\uparrow\rho}$, respectively, to the noise PSD using Fermi's golden rule:

$$\Gamma_{\downarrow\rho} = \chi^2\mathcal{S}_{nn}(\omega = \Omega) + \Gamma_1/4, \tag{2}$$

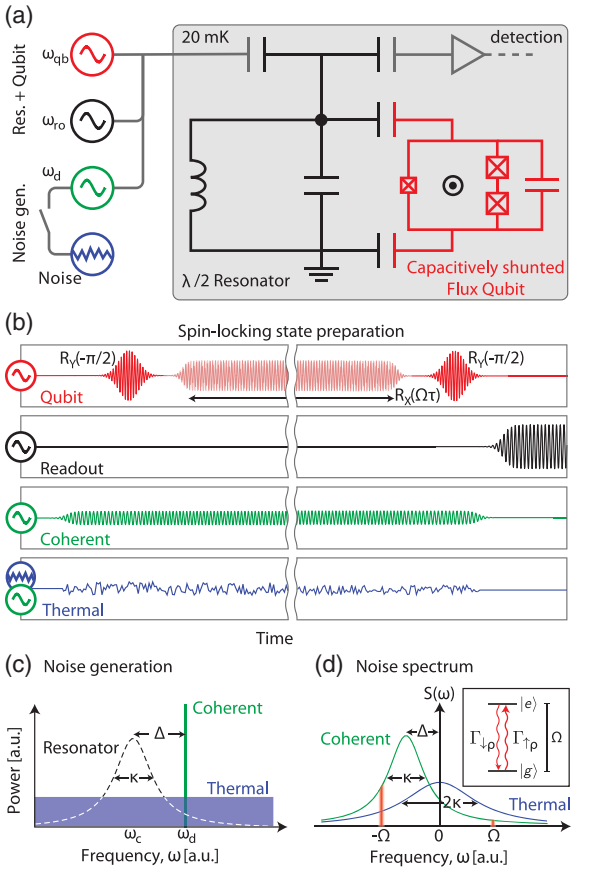

FIG. 1. Simplified measurement schematic and noise generation. (a) Device and measurement setup. A CSFQ is capacitively coupled to a $\lambda/2$ transmission line cavity. Besides qubit control (red) and readout (black) pulses, a weak, uniform, cavity drive (green) is applied to create a coherent state. To mimic thermal photon noise, we amplitude modulate this drive with a broadband white noise (blue). (b) Microwave implementation of the experiment. The qubit control sequence executes the spin-locking protocol, during which the photon noise generation signal is kept on. A strong readout pulse follows for dispersively measuring the qubit state. (c) Schematic diagram of coherent or thermal photon noise generation. The black curve indicates the cavity response. A single-frequency drive creates coherent photons in the cavity. A broadband noise (bandwidth $\gg \kappa$) mimics the thermal photon noise [32]. (d) Schematic of coherent or thermal photon noise spectrum. Coherent photons produce a noise spectrum symmetric with respect to $\omega = -\Delta$ and generally lead to unequal emission and absorption spectral densities (red bars) and, hence, unequal relaxation and excitation rates for the dressed qubit (inset). Thermal photons produce a symmetric spectrum, and the width is twice that of coherent photons.

$$\Gamma_{\uparrow\rho} = \chi^2\mathcal{S}_{nn}(\omega = -\Omega) + \Gamma_1/4, \tag{3}$$

where $\mathcal{S}_{nn}(\omega) = \int_{-\infty}^{\infty} d\tau e^{-i\omega\tau}\langle\hat{n}(0)\hat{n}(\tau)\rangle$ is the photon noise PSD. For simplicity, we will omit the subscript "nn" throughout the rest of the Letter. We emphasize that the fluctuating variable $\hat{n}$ is a quantum operator, and its

autocorrelation function $\mathcal{C}(\tau) = \langle \hat{n}(0)\hat{n}(\tau)\rangle$ may be complex or, equivalently, its Fourier transform asymmetric, $\mathcal{S}(\omega) \neq \mathcal{S}(-\omega)$. This is in contrast to classical noise, for which the above operator $\hat{n}$ is replaced with a classical variable n, such that $\mathcal{C}(\tau)$ is manifestly real and, thus, the power spectrum $\mathcal{S}(\omega) = \mathcal{S}(-\omega)$ is symmetric. In this work, the engineered noise from a coherent-state cavity photon serves as a nonequilibrium qubit environment, leading to an asymmetric photon noise spectrum. In contrast, for an environment in thermal equilibrium, the noise spectrum would be symmetric in the classical limit ($k_B T \gg \hbar\Omega$) and asymmetric in the quantum limit ($k_B T \ll \hbar\Omega$).

In the experiment, we engineer both coherent and thermal photon noise environments to study their differences [Fig. 1(c)]. Coherent photon noise is generated by sending a coherent tone at frequency ω_d ($\omega_d \sim \omega_c$) to drive and maintain a coherent state in the cavity. The corresponding photon-number correlation function is $\mathcal{C}^{\mathrm{coh}}(\tau) = \bar{n}e^{-i\Delta\tau-\kappa|\tau|/2} + \bar{n}^2$, where $\Delta = \omega_d - \omega_c$ is the frequency detuning of the coherent drive from the cavity [1,26]. Thermal photon noise is mimicked by generating a broadband white noise (bandwidth = 80 MHz) extending well beyond the cavity linewidth [15]. The corresponding photon-number correlation function is $\mathcal{C}^{\mathrm{th}}(\tau) = (\bar{n}^2 + \bar{n})e^{-\kappa|\tau|} + \bar{n}^2$ [33]. In the limit of small $\bar{n}$, these two correlation functions differ only by a factor of 2 in the correlation time. For coherent photons, the dominant term in the correlation function is the fluctuating field operator contracted with a coherent field—effectively a classical field—and the resulting correlation function decays at rate $\kappa/2$. In contrast, for the thermal photon noise case, the leading term is the contraction of the fluctuating field operator with itself, and this results in a correlation function with rate κ. This characteristic difference is also reflected in their corresponding Fourier transforms [Fig. 1(d)]:

$$\mathcal{S}^{\mathrm{coh}}(\omega) = \bar{n}\frac{\kappa}{(\omega+\Delta)^2 + (\kappa/2)^2}, \tag{4}$$

$$\mathcal{S}^{\mathrm{th}}(\omega) = (\bar{n}^2 + \bar{n})\frac{2\kappa}{\omega^2 + \kappa^2}, \tag{5}$$

for $\omega \neq 0$. Both spectra are Lorentzian shaped and increase with the mean photon number (linearly if $\bar{n} \ll 1$). There are two notable differences between Eqs. (4) and (5). First, the spectrum $\mathcal{S}^{\mathrm{coh}}(\omega)$ for coherent photons is centered around $\omega = -\Delta$, indicating an asymmetric noise spectrum and, hence, emission and absorption rates that are not equal to one another, in general. Second, the width of the spectral distribution with thermal photons is twice that with coherent photons (HWHM, κ vs $\kappa/2$), reflecting the difference in their correlation times. Note that Eqs. (4) and (5) are strictly valid only when the qubit dispersive shift is small relative to the cavity decay rate ($\chi \ll \kappa$). Theories addressing the generalized case are discussed in Refs. [14,34].

We perform spin-locking noise spectroscopy to measure the noise PSDs in the frequency range near the cavity decay rate κ. The implemented spin-locking pulse sequence comprises three pulses [Fig. 1(b)]. Following a $\pi/2$ pulse about the $-Y$ axis, a constant drive along the X axis locks the qubit state for a variable duration (conventional rotating-frame X/Y notation applies here). The locking X pulse also defines the dressed quantization axis [denoted by the z axis as in Eq. (1)]. The longitudinal polarization $\langle\sigma_z\rangle$ decays at rate $\Gamma_{1\rho} = \Gamma_{\downarrow\rho} + \Gamma_{\uparrow\rho}$ during the locking period. A final $\pi/2$ pulse about the Y axis projects the remaining polarization onto the measurement axis. By varying the length of the constant drive, we record the decay of the z polarization. Following Eqs. (2) and (3) and in the steady state, we have

$$\bar{\mathcal{S}}(\Omega) = \frac{\mathcal{S}(\Omega) + \mathcal{S}(-\Omega)}{2} = \frac{1}{2\chi^2}\left(\Gamma_{1\rho}(\Omega) - \frac{\Gamma_1}{2}\right), \tag{6}$$

$$\langle\sigma_z^{\mathrm{ss}}(\Omega)\rangle = \frac{\mathcal{S}(\Omega) - \mathcal{S}(-\Omega)}{\mathcal{S}(\Omega) + \mathcal{S}(-\Omega)}, \tag{7}$$

where $\bar{\mathcal{S}}(\omega) = \int_{-\infty}^{\infty} d\tau e^{-i\omega\tau}\frac{1}{2}\langle\hat{n}(0)\hat{n}(\tau) + \hat{n}(\tau)\hat{n}(0)\rangle$ is the symmetrized PSD (by definition) and $\langle\sigma_z^{\mathrm{ss}}(\Omega)\rangle$ is the steady-state z polarization. Therefore, the noise PSDs can be extracted from the $T_{1\rho}$ decay functions at experimentally feasible Rabi frequencies.

In noise measurements using a coherent driving state, we record the spin-locking decay [Fig. 2(a)] at various Rabi frequencies Ω and detunings Δ. The value of Ω for a given drive amplitude is determined in a separate Rabi experiment (not shown). The traces are fit to an exponential decay, allowing us to extract $\Gamma_{1\rho}(\Omega, \Delta)$, and hence $\bar{\mathcal{S}}(\Omega, \Delta)$ and $\langle\sigma_z^{\mathrm{ss}}(\Omega, \Delta)\rangle$. Note that the generated noise spectrum is also parametrized by Δ, as indicated by the second argument. Using Eq. (6), the decay constant is converted to $\bar{\mathcal{S}}(\Omega, \Delta)$ and plotted in Fig. 2(b). Since $\bar{\mathcal{S}}(\omega)$ is symmetric by definition, it is sufficient to show only its values at positive frequencies. The steady-state polarization for various Ω and Δ is plotted in Fig. 2(c). Significant deviations from zero polarization suggests unequal relaxation and excitation rates. For the case of a blue-detuned drive ($\Delta \equiv \omega_d - \omega_c > 0$, case A in Fig. 2), the dressed qubit decays to a steady state closer to its excited state, meaning $\Gamma_{\downarrow\rho} < \Gamma_{\uparrow\rho}$ and the qubit tends to absorb energy from its environment. In contrast, the red-detuned case ($\Delta \equiv \omega_d - \omega_c < 0$, case C) saturates closer to the ground state, meaning $\Gamma_{\downarrow\rho} > \Gamma_{\uparrow\rho}$ and the qubit predominantly emits energy to its environment. This effect was demonstrated to stabilize the qubit in a pure state (here, its ground state) [30], an alternative approach to creating a

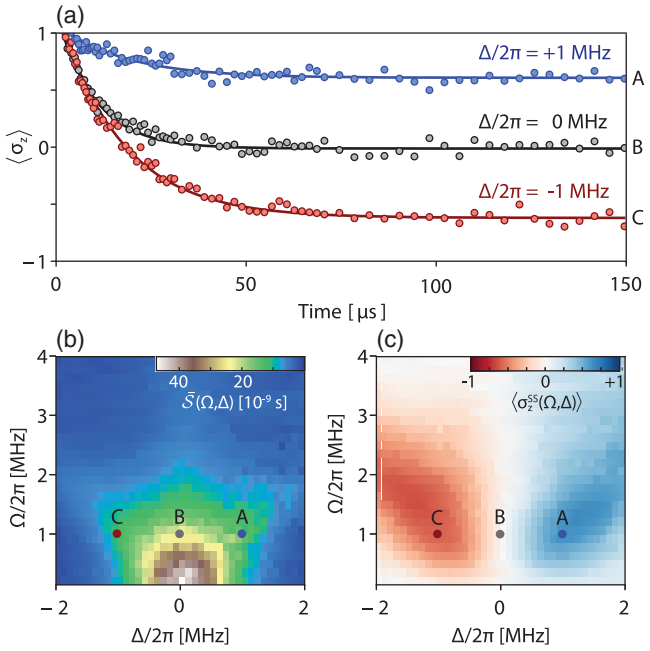

FIG. 2. $T_{1\rho}$ decay characterization. (a) $T_{1\rho}$ decay with coherent photons. The selected traces are measured at cavity drive detuning $\Delta/2\pi = +1$, 0, -1 MHz, respectively, and with the same cavity and qubit drive power ($\Omega/2\pi = 1$ MHz). The solid lines are exponential fits. (b) Symmetrized noise PSD with coherent photons vs. Ω and Δ, derived from the fitted decay constants by using Eq. (6). The markers denote the cases shown in (a). (c) Steady-state polarization with coherent photons vs Ω and Δ, extracted directly from the fit. The color scale, blue (red), indicates that the dressed qubit predominantly emits (absorbs) energy.

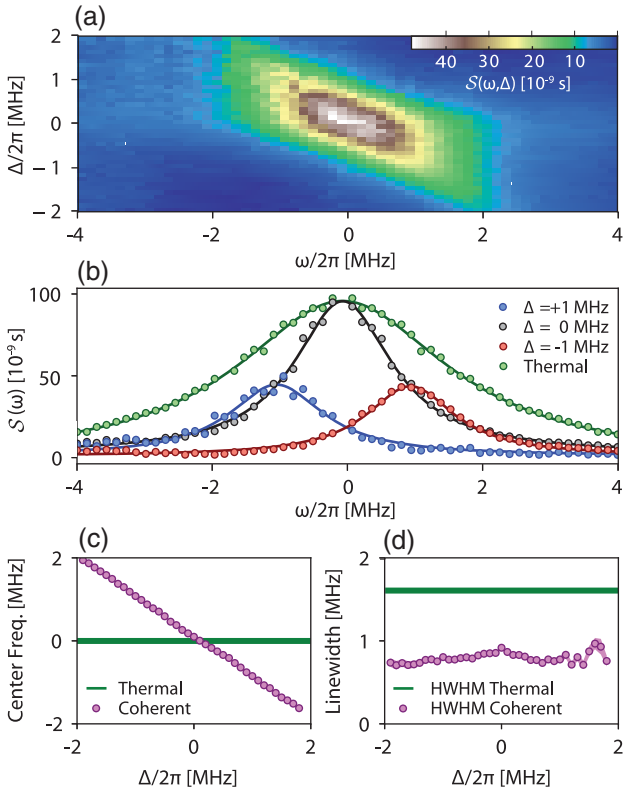

FIG. 3. Coherent and thermal photon noise spectra. (a) Two-sided (nonclassical) PSD $\mathcal{S}(\omega, \Delta)$ with coherent photons at various Δ, reconstructed from data shown in Figs. 2(b) and 2(c). (b) Example slices of reconstructed $\mathcal{S}(\omega)$. Plotted are three typical cases with coherent drive at $\Delta/2\pi = +1$, 0, -1 MHz and one thermal case which has no Δ dependence. The solid lines are Lorentzian fits. (c) Extracted center frequencies in both coherent and thermal cases. (d) Extracted HWHMs. The mean value of HWHMs with coherent photons is 0.83 MHz. The HWHM with thermal photons is 1.61 MHz. The green lines in (c) and (d) are included as a guide to the eye, since the thermal photons are generated with broadband noise and have no Δ dependence.

nonequilibrium effective qubit temperature low enough to reach the quantum limit ($T_{\text{eff}} \ll \Omega$).

The above features are apparent in the reconstructed spectra $\mathcal{S}(\omega)$ shown in Figs. 3(a) and 3(b), which are derived from Eqs. (6) and (7) at $\omega = \pm\Omega$ using the data from Fig. 2 and may, in principle, be nonclassical. First, the smooth and continuous transition around $\omega = 0$ indicates that our spectroscopy methods correctly connect positive and negative frequencies. The tilted square pattern in the 2D spectrum $\mathcal{S}(\omega, \Delta)$ also indicates that the spectral peak moves with Δ. The peak amplitude is reduced when moving away from zero frequency for the same drive power, as the mean photon number becomes smaller ($\bar{n} \propto [1/\Delta^2 + (\kappa/2)^2]$). Figures 3(c) and 3(d) show that the extracted Lorentzian center frequencies for coherent photons follow $\omega = -\Delta$, and the HWHMs ($\approx$0.83 MHz) are approximately half that of the corresponding measurement for thermal photons ($\approx$1.61 MHz). Such a factor of 2 difference in the spectral width is a major feature that can be used for differentiating coherent and thermal photon sources. We note that the width difference is not exactly twice, due to the small yet non-negligible perturbation from the qubit ($\chi/\kappa \approx 0.18$), which shifts the cavity response depending on the qubit state [14]. The experimental results agree with Eqs. (4) and (5), validating our approach.

We implemented the same technique on a second device with a similar design. The device was measured with $\omega_c/2\pi = 8.27$ GHz, $\kappa/2\pi = 1.5$ MHz, $\chi/2\pi = 0.45$ MHz, $\omega_q/2\pi = 4.7$ GHz, $T_1 = 35$–55 μs, and $T_{2\text{Echo}} = 40$ μs [9]. Figure 4(a) shows the spin-locking noise-spectroscopy results, which again demonstrate the characteristic factor of 2 difference between the HWHMs of injected coherent and thermal photons. We also found that the spectrum measured without added noise (blue) has a -3 dB point consistent with thermal photon noise. Therefore, we suspected that thermal radiation from higher-temperature stages in the DR was responsible for the residual cavity photons and the resulting dephasing. By measuring the dependence of the dephasing rate on the average number of engineered thermal-noise photons, we extrapolated the average residual thermal photon number in the absence of externally applied noise to

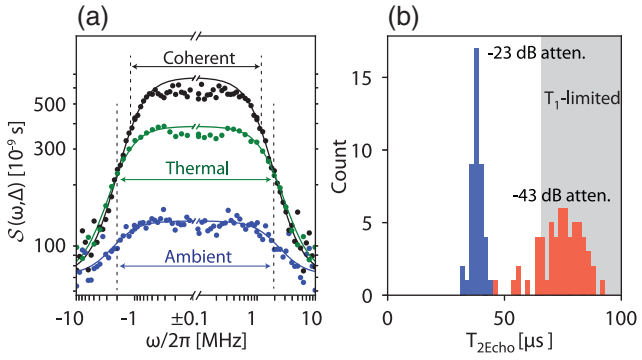

FIG. 4. Decoherence mitigation. (a) Photon noise spectra with the second device. Plotted are spectra with injected coherent photons (black), injected thermal photons (green), and no injected photons (blue). Solid lines are a Lorentzian fit. Arrows indicate the peak width spanned by the corresponding −3 dB points (dashed lines) for the thermal and ambient cases (HWHM ≈ 2.0 MHz) and for the coherent case (HWHM ≈ 1.1 MHz). Because the injected noise disrupts the spin-locking condition when the locking drive is weak, the measured PSDs at the low-frequency end (< 0.4 MHz) are consistently lower and, hence, excluded during fitting. (b) Histogram of measured $T_{2\mathrm{Echo}}$ statistics before and after adding extra attenuation on the input side of the cavity. In both cases, the fluctuation mainly comes from temporal T_1 instability due to quasiparticles [37]. The gray area indicates the spread of the $2T_1$ limit measured with −43 dB attenuation.

be around 0.006, corresponding to an 80 mK equilibrium temperature [9]. During a subsequent thermal cycling of the dilution fridge, we increased the attenuation at the mixing chamber (20 mK) from 23 to 43 dB in order to reduce the thermal photons reaching the cavity (see details in Supplemental Material [35]). This modification significantly increased $T_{2\mathrm{Echo}}$ to 80 μs [Fig. 4(b)], while T_1 did not change. The new attenuator configuration effectively suppresses the residual thermal photons in our cavity to $\bar{n} < 0.0006$ [35], 10 times lower than the previous level. This corresponds to an equivalent equilibrium temperature of 55 mK. Because of the temporal spread of coherence times and measurement uncertainty, we could not confirm a lower bound, though measurements of the excited-state population of several qubits tested in the same dilution fridge found an effective temperature of 35 mK [36].

In conclusion, we developed a spin-locking ($T_{1\rho}$) technique for performing nonclassical noise spectroscopy and demonstrated it using engineered photon noise applied to a superconducting circuit QED system. The measured noise spectra were used to distinguish between coherent and thermal cavity photon noise. Using this technique, we found that residual thermal photons limit our qubit coherence. By adding attenuation at the lowest temperature stage, we successfully reduced the residual thermal photon number and recovered $T_{2\mathrm{Echo}} \approx 2T_1$. Further improvement may be possible with more careful choice of attenuator or filter configuration or active cooling techniques.

We thank Alexandre Blais, Lorenza Viola, Jan Goetz, and Michael Marthaler for insightful discussions. We thank Mirabella Pulido and Hongcheng Sun for generous assistance. This research was funded in part by the Office of the Director of National Intelligence (ODNI), Intelligence Advanced Research Projects Activity (IARPA) and by the Assistant Secretary of Defense for Research and Engineering via MIT Lincoln Laboratory under Air Force Contract No. FA8721-05-C-0002; by the U.S. Army Research Office Grant No. W911NF-14-1-0682; and by the National Science Foundation Grant No. PHY-1415514. M. K. gratefully acknowledges support from the Carlsberg Foundation. The views and conclusions contained herein are those of the authors and should not be interpreted as necessarily representing the official policies or endorsements, either expressed or implied, of ODNI, IARPA, or the U.S. Government.

F. Y. and D. C. contributed equally to this work.

*fyan@mit.edu

[1] A. Blais, R.-S. Huang, A. Wallraff, S. M. Girvin, and R. J. Schoelkopf, Phys. Rev. A **69**, 062320 (2004).
[2] J. Majer, J. Chow, J. Gambetta, J. Koch, B. Johnson, J. Schreier, L. Frunzio, D. Schuster, A. Houck, A. Wallraff, A. Blais, M. H. Devoret, S. M. Girvin, and R. J. Schoelkopf, Nature (London) **449**, 443 (2007).
[3] M. A. Sillanpää, J. I. Park, and R. W. Simmonds, Nature (London) **449**, 438 (2007).
[4] R. W. Heeres, P. Reinhold, N. Ofek, L. Frunzio, L. Jiang, M. H. Devoret, and R. J. Schoelkopf, Nat. Commun. **8**, 94 (2017).
[5] D. I. Schuster, A. Wallraff, A. Blais, L. Frunzio, R.-S. Huang, J. Majer, S. M. Girvin, and R. J. Schoelkopf, Phys. Rev. Lett. **94**, 123602 (2005).
[6] A. A. Houck, J. A. Schreier, B. R. Johnson, J. M. Chow, J. Koch, J. M. Gambetta, D. I. Schuster, L. Frunzio, M. H. Devoret, S. M. Girvin, and R. J. Schoelkopf, Phys. Rev. Lett. **101**, 080502 (2008).
[7] A. P. Sears, A. Petrenko, G. Catelani, L. Sun, H. Paik, G. Kirchmair, L. Frunzio, L. I. Glazman, S. M. Girvin, and R. J. Schoelkopf, Phys. Rev. B **86**, 180504 (2012).
[8] C. Rigetti, J. M. Gambetta, S. Poletto, B. L. T. Plourde, J. M. Chow, A. D. Córcoles, J. A. Smolin, S. T. Merkel, J. R. Rozen, G. A. Keefe, M. B. Rothwell, M. B. Ketchen, and M. Steffen, Phys. Rev. B **86**, 100506 (2012).
[9] F. Yan, S. Gustavsson, A. Kamal, J. Birenbaum, A. P. Sears, D. Hover, T. J. Gudmundsen, D. Rosenberg, G. Samach, S. Weber, J. L. Yoder, T. P. Orlando, J. Clarke, A. J. Kerman, and W. D. Oliver, Nat. Commun. **7**, 12964 (2016).
[10] K. Y. Tan, M. Partanen, R. E. Lake, J. Govenius, S. Masuda, and M. Möttönen, Nat. Commun. **8**, 15189 (2017).
[11] C. C. Bultink, M. A. Rol, T. E. O'Brien, X. Fu, B. C. S. Dikken, C. Dickel, R. F. L. Vermeulen, J. C. de Sterke, A. Bruno, R. N. Schouten, and L. DiCarlo, Phys. Rev. Applied **6**, 034008 (2016).

[12] D. T. McClure, H. Paik, L. S. Bishop, M. Steffen, J. M. Chow, and J. M. Gambetta, Phys. Rev. Applied **5**, 011001 (2016).
[13] J.-H. Yeh, J. LeFebvre, S. Premaratne, F. Wellstood, and B. Palmer, J. Appl. Phys. **121**, 224501 (2017).
[14] J. Gambetta, A. Blais, D. I. Schuster, A. Wallraff, L. Frunzio, J. Majer, M. H. Devoret, S. M. Girvin, and R. J. Schoelkopf, Phys. Rev. A **74**, 042318 (2006).
[15] D. I. Schuster, A. A. Houck, J. A. Schreier, A. Wallraff, J. M. Gambetta, A. Blais, L. Frunzio, J. Majer, B. Johnson, M. H. Devoret, S. M. Girvin, and R. J. Schoelkopf, Nature (London) **445**, 515 (2007).
[16] M. Hofheinz, E. Weig, M. Ansmann, R. C. Bialczak, E. Lucero, M. Neeley, A. O'connell, H. Wang, J. M. Martinis, and A. Cleland, Nature (London) **454**, 310 (2008).
[17] J. Goetz, S. Pogorzalek, F. Deppe, K. G. Fedorov, P. Eder, M. Fischer, F. Wulschner, E. Xie, A. Marx, and R. Gross, Phys. Rev. Lett. **118**, 103602 (2017).
[18] R. J. Schoelkopf, A. A. Clerk, S. M. Girvin, K. W. Lehnert, and M. H. Devoret, in *Quantum Noise in Mesoscopic Physics*, edited by Y. V. Nazarov (Springer Netherlands, Dordrecht, 2003), pp. 175–203.
[19] O. Astafiev, Y. A. Pashkin, Y. Nakamura, T. Yamamoto, and J. S. Tsai, Phys. Rev. Lett. **93**, 267007 (2004).
[20] R. C. Bialczak, R. McDermott, M. Ansmann, M. Hofheinz, N. Katz, E. Lucero, M. Neeley, A. D. O'Connell, H. Wang, A. N. Cleland, and J. M. Martinis, Phys. Rev. Lett. **99**, 187006 (2007).
[21] J. Bylander, S. Gustavsson, F. Yan, F. Yoshihara, K. Harrabi, G. Fitch, D. G. Cory, Y. Nakamura, J.-S. Tsai, and W. D. Oliver, Nat. Phys. **7**, 565 (2011).
[22] G. A. Álvarez and D. Suter, Phys. Rev. Lett. **107**, 230501 (2011).
[23] F. Yan, J. Bylander, S. Gustavsson, F. Yoshihara, K. Harrabi, D. G. Cory, T. P. Orlando, Y. Nakamura, J.-S. Tsai, and W. D. Oliver, Phys. Rev. B **85**, 174521 (2012).
[24] F. Yoshihara, Y. Nakamura, F. Yan, S. Gustavsson, J. Bylander, W. D. Oliver, and J.-S. Tsai, Phys. Rev. B **89**, 020503 (2014).
[25] F. Yan, S. Gustavsson, J. Bylander, X. Jin, F. Yoshihara, D. G. Cory, Y. Nakamura, T. P. Orlando, and W. D. Oliver, Nat. Commun. **4**, 2337 (2013).
[26] A. A. Clerk, M. H. Devoret, S. M. Girvin, F. Marquardt, and R. J. Schoelkopf, Rev. Mod. Phys. **82**, 1155 (2010).
[27] C. M. Quintana, Y. Chen, D. Sank, A. G. Petukhov, T. C. White, D. Kafri, B. Chiaro, A. Megrant, R. Barends, B. Campbell, Z. Chen, A. Dunsworth, A. G. Fowler, R. Graff, E. Jeffrey, J. Kelly, E. Lucero, J. Y. Mutus, M. Neeley, C. Neill *et al.*, Phys. Rev. Lett. **118**, 057702 (2017).
[28] G. A. Paz-Silva, L. M. Norris, and L. Viola, Phys. Rev. A **95**, 022121 (2017).
[29] E. Collin, G. Ithier, A. Aassime, P. Joyez, D. Vion, and D. Esteve, Phys. Rev. Lett. **93**, 157005 (2004).
[30] K. W. Murch, U. Vool, D. Zhou, S. J. Weber, S. M. Girvin, and I. Siddiqi, Phys. Rev. Lett. **109**, 183602 (2012).
[31] M. Loretz, T. Rosskopf, and C. L. Degen, Phys. Rev. Lett. **110**, 017602 (2013).
[32] R. Loudon, *The Quantum Theory of Light* (Oxford University, New York, 2000).
[33] P. Bertet, I. Chiorescu, C. Harmans, and J. Mooij, arXiv: cond-mat/0507290.
[34] A. A. Clerk and D. W. Utami, Phys. Rev. A **75**, 042302 (2007).
[35] See Supplemental Material at http://link.aps.org/supplemental/10.1103/PhysRevLett.120.260504 for a description of the changes to the microwave setup, our theoretical motivation for making those changes, and a derivation of the spectrum of photon noise in the cavity.
[36] X. Y. Jin, A. Kamal, A. P. Sears, T. Gudmundsen, D. Hover, J. Miloshi, R. Slattery, F. Yan, J. Yoder, T. P. Orlando, S. Gustavsson, and W. D. Oliver, Phys. Rev. Lett. **114**, 240501 (2015).
[37] S. Gustavsson, F. Yan, G. Catelani, J. Bylander, A. Kamal, J. Birenbaum, D. Hover, D. Rosenberg, G. Samach, A. P. Sears, S. J. Weber, J. L. Yoder, J. Clarke, A. J. Kerman, F. Yoshihara, Y. Nakamura, T. P. Orlando, and W. D. Oliver, Science **354**, 1573 (2016).